Review

Received: 18 February 2022 Revised: 31 March 2022 Accepted article published: 10 April 2022 Published online in Wiley Online Library:

(wileyonlinelibrary.com) DOI 10.1002/pi.6402

Polyhydroxybutyrate: a review of experimental and simulation studies of the effect of fillers on crystallinity and mechanical properties

Katarzyna Majerczak,[a†] Dominic Wadkin-Snaith,[b†] Vitor Magueijo,[b] Paul Mulheran,[b] John Liggat[a] and Karen Johnston[b*]

Abstract

Polyhydroxybutyrate (PHB) is a sustainable polymer that is a promising candidate for replacing petroleum-based plastics in food packaging. Fillers are used to improve the mechanical properties of PHB composites, simultaneously changing the crystallinity of the polymer matrix. However, it is not well understood how fillers affect crystallisation and microstructure, and thus the resulting mechanical properties of the composite. This review summarises simulation work on polymer nucleation and crystallisation and how nucleation is influenced by different types of polymer–filler interfaces. Experimental studies of PHB composites with a wide variety of fillers are reviewed to find trends between the filler type, crystallinity and mechanical properties. It is clear that fillers act as nucleants that increase the number of spherulites while reducing spherulite size. This behaviour is apparent for almost all fillers regardless of filler chemistry or topology. However, the data obtained from the literature do not seem to produce strong conclusions about the effect of the degree of crystallinity on the tensile properties of PHB–filler composites, although there are some weak trends that indicate the importance of microstructure. In order to enable prediction and control of PHB composite properties, further systematic studies are required to elucidate the effect of specific filler types and the connection between crystallinity, microstructure and mechanical properties.

Supporting information may be found in the online version of this article.

INTRODUCTION

Plastic pollution has become an urgent problem in contemporary society. The amount of plastic produced from 2004 to 2018 was equal to that produced in the previous half century, of which the vast majority (*ca*. 80%) was sent to landfill or directly released to the environment.[1] This in turn leads to microplastic pollution, affecting wildlife and entering the human food chain via drinking water,[2] foodstuffs[3] or air.[4] In addition to plastic pollution, plastics commonly used in industry are derived from unsustainable sources (i.e. petrochemicals), emphasising the need for their replacement with sustainably sourced alternatives. Ideally, society must reduce plastic use, and recycle when possible. However, in some cases, plastic can play a valuable role in reducing emissions, such as thin films for food packaging that reduces food waste, a major emitter of greenhouse gases.[5,6] Plastic films are often not recyclable, due to infrastructure limitations. In this case, the plastic food packaging film should be compostable either in an anaerobic digestion plant that can generate energy or, if it goes to landfill, by breaking down without the creation of harmful microplastics. Promising sustainable and compostable polymers include alginate sourced from seaweed, cellulose sourced from agricultural waste and polyhydroxyalkanoates (PHAs) which can be sourced from bacterial fermentation of food or agricultural waste. PHAs are of particular interest as they can be melt-processed, making them compatible with existing manufacturing processes. They can be naturally synthesised by a variety of microorganisms via the formation of polyhydroxyesters from short- or medium-chain hydroxyalkanoic acids.[7,8] Because of variations in the degree of polymerisation, the position of the hydroxyl group, the chemistry of constituent monomers in copolyesters[9] and the process conditions under which they can be manufactured, so far over 150 different types of PHA polymers have been reported.[10,11]

These different types of PHAs yield different material properties,[12–17] and can possess properties similar to those of traditional thermoplastics such as polyethylene and polypropylene[18] including oxygen and water barrier properties,[19] all while maintaining biodegradability.[20] However, the desired properties are difficult

* *Correspondence to: Karen Johnston, Department of Chemical and Processing Engineering, James Weir Building, 75 Montrose Street, University of Strathclyde, Glasgow G1 1XJ, UK. E-mail: karen.johnston@strath.ac.uk*

† *These authors contributed equally.*

a *Department of Pure and Applied Chemistry, University of Strathclyde, Glasgow, UK*

b *Department of Chemical and Processing Engineering, University of Strathclyde, Glasgow, UK*

to obtain simultaneously and have not been optimised for particular applications. Many of these properties are linked to the crystallinity and morphology of the PHA, and thus control over the crystallinity and microstructure could be used to further tune the properties of PHAs.

PHAs exhibit a semicrystalline multiscale structure, as shown schematically in Fig. 1 for the particular case of polyhydroxybutyrate (PHB). At small length scales, polymer chains align to form crystalline lamella structures where the chains extend from the crystalline region and can fold back into the crystal, or become embedded in an amorphous region between the lamellae. The lamellae in turn are layered into microfibrils which grow outward in a radial manner to form spherulites (Fig. 1). In order to achieve reproducible polymer properties, it is essential to carefully control both the process conditions (temperature, feedstock purity, addition of additives) and ageing (storage time and environmental conditions) as they significantly influence the overall crystallinity and film morphology.

PHB is the most broadly studied PHA[22,23] and exists as an amorphous polymer *in vivo*.[24] Upon application of a physical treatment, e.g. drying, coalescence of PHB inclusions takes place, resulting in homogeneous nucleation[25] and crystallisation.[26] PHB produced by bacteria is isotactic (all the repeat units have the same stereochemical configuration).[27,28] While many studies have investigated changes in PHB crystallinity due to changes in environmental conditions,[29,30] the introduction of additives[31,32] or processing steps,[33] there is little understanding of how fillers affect the kinetics and mechanism of crystallisation. Consequently, there is a gap in the ability to control the microstructure to ensure reproducible barrier, mechanical and optical properties of PHB plastics.[19] To gain understanding of how filler addition influences crystallisation, it is necessary to study how the filler surface induces nucleation. While experimental characterisation of the interfacial region is challenging, simulations are a valuable tool in investigating the interfacial properties of the filler–polymer matrix, as they provide molecular-level insight into polymer crystal nucleation mechanisms.[34]

In this review, we focus on how filler addition influences the crystallinity of PHB. We first give a brief overview of some relevant experimental characterisation methods, alongside molecular simulation techniques used to simulate polymer crystal nucleation and growth. We then review simulations of generic polymer crystal nucleation, and the experimentally observed formation and growth of crystals in pure PHB. Next, we review simulation studies of generic polymer crystal nucleation at various filler surfaces. Finally, we look at experimental results on how the addition of filler particles impacts crystallinity, spherulite size and mechanical properties in PHB composites. The combination of experimental data and simulation studies provides new insight into polymer crystallisation, which will enable the prediction of how fillers affect PHB crystallinity, and thus facilitate the design of plastic films for food packaging applications.

OVERVIEW OF RELEVANT EXPERIMENTAL AND SIMULATION TECHNIQUES

Polymer crystal, lamellar and spherulitic structures and degree of crystallinity, X_c, are typically characterised using a range of techniques, including XRD, Fourier transform infrared (FTIR) spectroscopy, DSC and polarised light microscopy. XRD methods including wide-angle X-ray diffraction, small-angle X-ray scattering (SAXS) and grazing incidence SAXS (GISAXS) are widely used techniques for investigating the degree of crystallinity and are considered to be the most reliable methods used for this purpose.[35] Despite the complexity of the analysis, these techniques provide absolute values of X_c unlike the relative values obtained from FTIR spectroscopy and DSC measurements. The mechanical properties of PHB-based composites are often characterised using Young's modulus (E), tensile strength (σ) and strain at break (ε_b) of the composites, and for conciseness and clarity, these properties are defined in Fig. 2.

Classical molecular dynamics (MD) is a computational method for simulating systems of particles, which are typically characterised by their mass and their interactions with other particles.

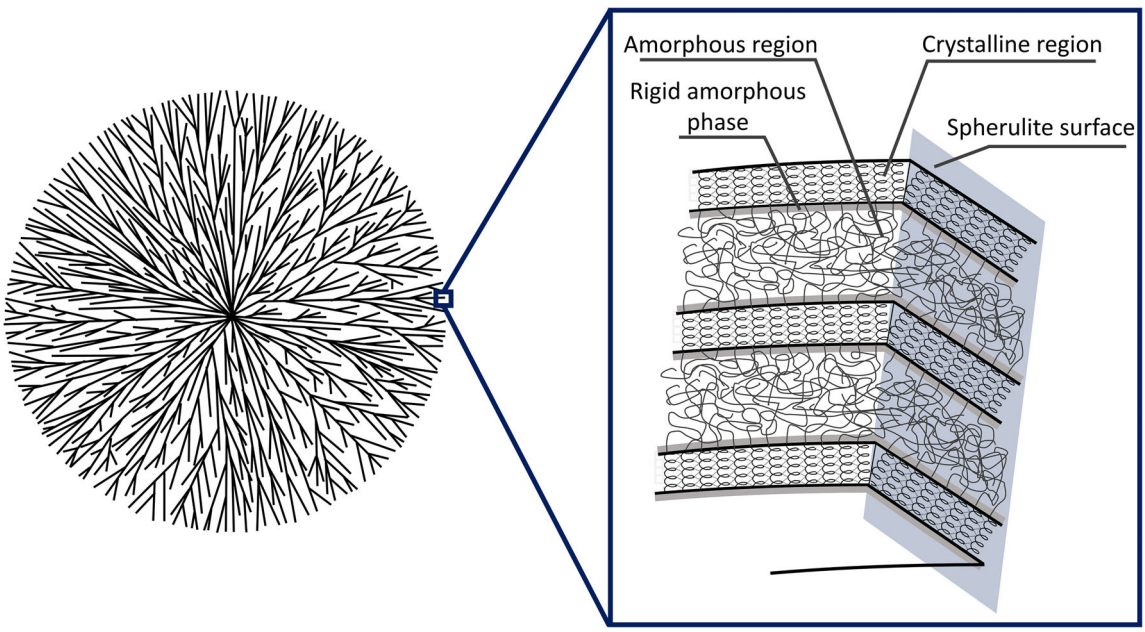

Figure 1. Schematic diagram of a PHB spherulite consisting of microfibrils and lamellae. Adapted from Dingler *et al.*[21]

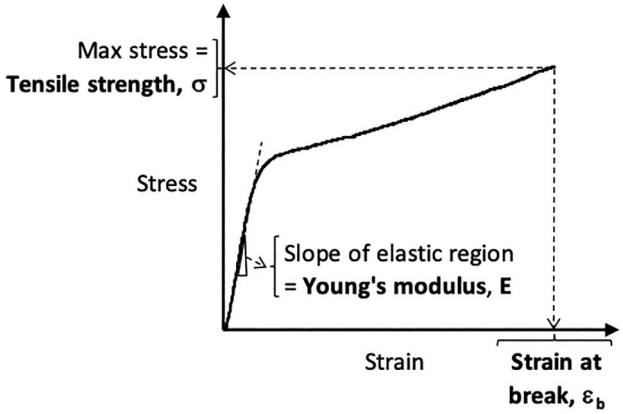

Figure 2. Typical stress *versus* strain (elongation) curve obtained by tensile testing and definition of Young's modulus, tensile strength and strain at break.

Starting from known particle positions and velocities, Newton's laws are solved numerically to obtain particle trajectories. By averaging the system properties over time it is possible to obtain useful information about a material such as density, melting temperature, glass transition temperature, scattering data, etc. The thermodynamic behaviour of a system can also be studied using Monte Carlo (MC) techniques, which generate new configurations for the system by making random changes to the system degrees of freedom (e.g. particle positions), thus generating low-energy configurations for the system of study. For comprehensive descriptions of the MD and MC methods we refer the reader to standard textbooks.[36,37]

In both of these simulation methods, the systems can be represented at different length scales, depending on whether the particles represent individual atoms, groups of atoms or have no chemical specificity, as illustrated in Fig. 3. An atomistic model of PHB explicitly represents all carbon, oxygen and hydrogen atoms. While atomistic models retain chemical specificity, they can be time-consuming to run and are often limited to systems of oligomers and times up to hundreds of nanoseconds. To access longer time scales and simulate longer chains, coarse-grained (CG) models can be used. Coarse-graining is the practice of removing degrees of freedom whilst retaining enough chemical detail to reproduce the characteristics of the atomistic model, such as density. The united atom (UA) model is an example of a CG model that combines a carbon atom with its bonded hydrogens to form one 'atom' or 'bead'. For polymers, it is beneficial to use coarser models, for example representing a monomer with one, two or four beads, etc.[38–41] Even longer time scales and polymer chains can be reached using generic polymer (bead–spring) models, such as the Kremer–Grest model.[42] The Kremer–Grest model exhibits typical polymer properties, including glass transition, entanglement effects and reduced entanglement moduli.[43] Since many of the dynamic phenomena displayed by these models are characteristic of whole classes of polymer, these models can be mapped to real polymers,[43,44] including PHAs.

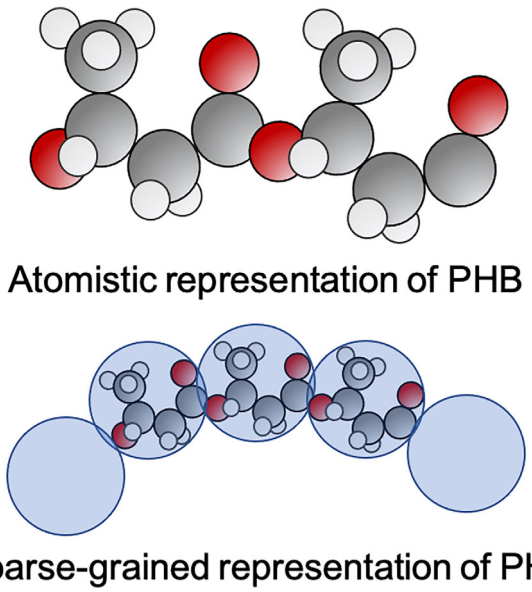

Figure 3. Atomistic model (top) and CG model (bottom) of PHB. Red, grey and white spheres correspond to oxygen, carbon and hydrogen atoms, respectively. In this schematic, each blue CG bead represents one PHB monomer.

CRYSTALLISATION IN PURE PHB AND COMPARISON OF CRYSTALLISATION IN GENERIC POLYMER MODELS

PHB is a semicrystalline polymer that, similar to other linear polymers, forms lamellae that arrange into multilamellar structures (microfibrils) that further assemble into spherulites (Fig. 1). In this section we review experimental studies of PHB and simulations of generic/CG polymer models to describe the crystallisation process in PHB, including crystal nucleation, growth of nuclei into lamellae, and lamellae and spherulite structure. Finally, we briefly discuss the amorphous regions connecting the crystalline domains.

PHB crystal structure and nucleation

The thickness of a single PHB crystal is typically 4–10 nm depending on the polymer molecular weight (M_w) and processing conditions.[15,45,46] The crystalline structure has two polymorphs, α and β, which have been previously described in detail.[47–50] The α-form corresponds to a helical structure in anti-parallel orientation,[49] with two chains (four monomeric units) contained in an orthorhombic $P2_12_12_1$ unit cell.[51] The individual helical structures interact with the adjacent chains via C—H···O═C hydrogen bonding.[52] The structure of the α-form is shown in Fig. 4 and the lattice parameters are presented in Table 1. The conformation of the β-form is much less clear and remains the subject of scientific discussion as both orthorhombic and hexagonal conformations (Table 1) have been reported. In contrast, more recent studies have proposed that the β-form consists of a non-crystalline (albeit X-ray active), highly oriented mesophase.[53] In general, β-form crystals can be created by uniaxial stretching of a PHB film, via a transformation from the α-form (a metastable, reversible process), or from arrangement of constrained amorphous regions between small crystallites in the matrix.[48,54]

Currently, there are very few atomistic and CG simulations of PHB,[55–57] and these do not address crystallisation of PHB. However, there are studies of polymer crystallisation using generic/CG models that capture the general physics of polymer crystallisation. We expect simulations of crystallisation from the melt using these models to be relevant to the crystallisation behaviour of PHAs, although we note that the crystal structure of these models will be different from that of PHB. Hexagonal crystal symmetry has

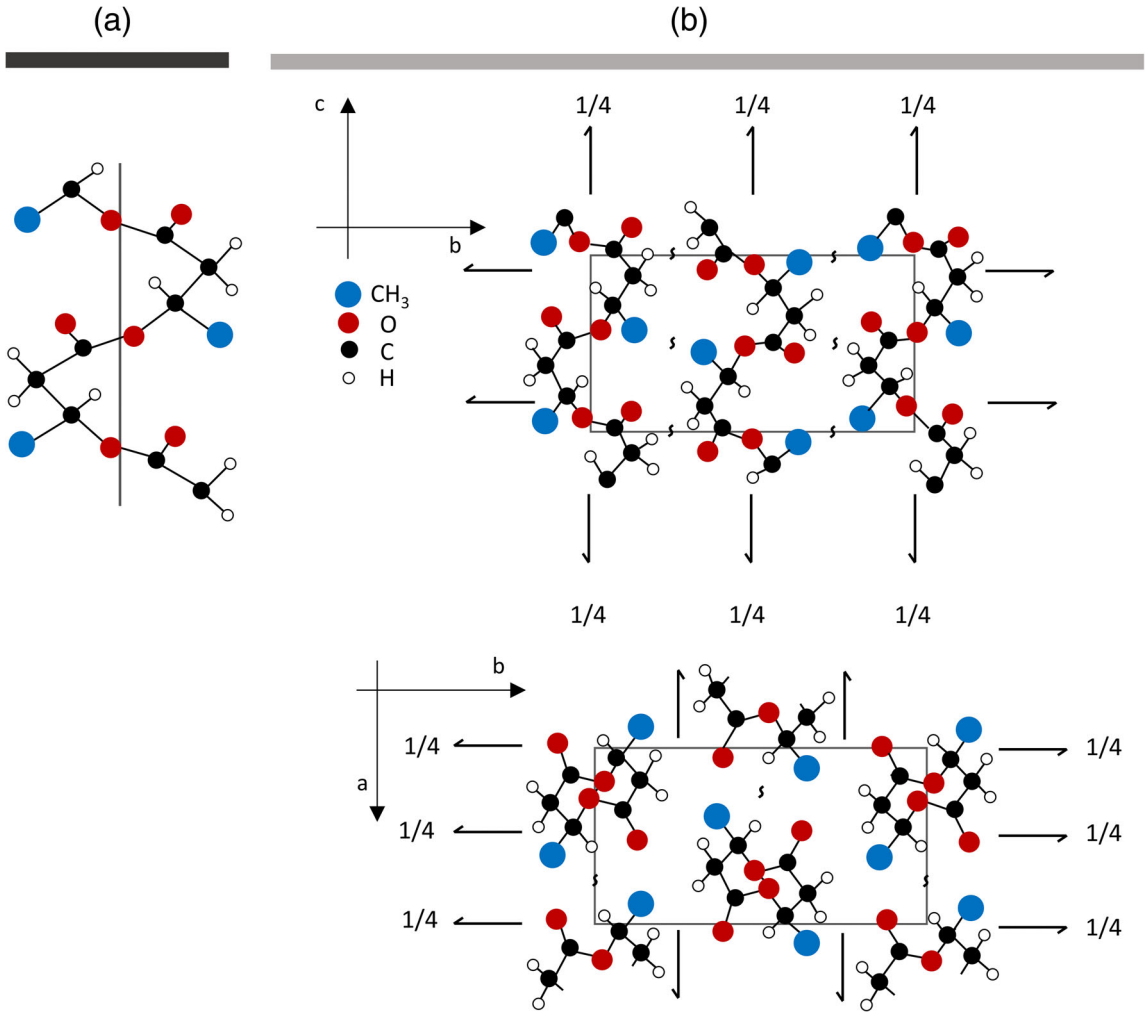

Figure 4. Crystal structure of the PHB α-form: (a) direction normal to the helix axis; (b) projection of the PHB single cell in *c*–*b* and *a*–*b* planes, where the latter corresponds to the direction along the helical axis. Adapted from Wang and Tashiro.[68]

Table 1. Crystallographic data and lattice parameters for the α- and β-forms of PHB

Form	Lattice	Space group	*a* (Å)	*b* (Å)	*c* (Å)	Ref.
α	Orthorhombic	$P2_12_12_1$-D_2^4	5.73	13.15	5.93	69
α	—	$P2_12_12_1$-D_2^4	5.76	13.20	5.96	49
β	Orthorhombic	—	5.28	9.20	4.69	70–72
β	Orthorhombic	$P2_12_12_1$	5.76	13.2	5.98	48
β	Hexagonal	$P3_221$	9.22	—	4.66	69

been observed in studies using UA, CG and generic polymer models[38,58–63] and appears to be a common feature of these models. However, some studies using various generic polymer models observed both hexagonal close packed and face-centred cubic regions,[64–66] while another study found an orthorhombic structure to be energetically favourable.[67]

Nucleation of crystals is believed to be facilitated by hydrogen bonding that reduces chain mobility, enabling closer chain packing.[73,74] One of the advantages of simulations over experiments is the ability to gain insight into the molecular origins of polymer crystal nucleation and the size of the critical nucleus, which is the smallest ordered structure that gives rise to a thermodynamically stable crystal. Yi and Rutledge[60,75] performed MC and MD simulations using a UA model for alkanes, and found critical nuclei sizes of 23 ± 3 and 126 beads for systems of 8-bead and 20-bead oligomers, respectively. Within these studies, melting temperatures of 212 ± 2 and 310 ± 2 K for the 8- and 20-bead systems, respectively, agreed well with the respective experimental values of 216.4 and 309.8 K. The size of the critical nucleus was found to decrease the further below the melt temperature the simulation was carried out. A more recent study[76] using a similar UA model with 20-bead oligomers used a different analysis method and found a critical nucleus size of 80 beads ±25%. The discrepancy in these results highlights an ambiguity in the way the critical nucleus is defined and on the analytical method deployed.

The above studies gave an estimate of the size of a critical nucleus; however, they did not investigate the molecular mechanisms that give rise to the formation of an ordered crystal nucleus from a polymer melt. In one crystal nucleation study, Takeuchi[77] quenched a melt of 20-bead UA chains from well above the glass transition temperature and tracked the ordering of the system using the structure factor and local orientational order. Local parallel order (chain straightening and alignment) in the induction period led to ordered clusters, causing density fluctuations that were seen in the structure factor, which the author noted were found in experimental studies of crystallisation in poly(ethylene terephthalate) using SAXS measurements. A study of semi-rigid chains also found that local order occurred on short time scales, followed by densification.[78]

Anwar *et al.*[76] also investigated the microscopic mechanisms driving the formation of a critical nucleus. They quenched a UA 20-bead model and then tracked several observables including radius of gyration, nematic order parameter and a crystallinity order parameter for candidate nucleus structures. At early times there is an increase in global order signifying chain alignment. This is followed by densification and chain straightening. Finally, local positional and orientational order is established. The authors note that this modifies the conclusions made in previous studies.[77,78] Anwar and Schilling[61] used the UA model to study 500-bead chains and observed the same mechanism as for the shorter chains.[76] This more recent simulation picture of critical nucleus formation has also been seen in MC studies,[62] where it is deduced that the orientational order between straight-chain segments drives crystal nucleation.

Lamella formation and growth

While the critical nucleus size, crystal structure and molecular mechanisms driving the formation of a critical nucleus are amenable to simulations using short chains, at this length true lamella structures that contain folded chains cannot form (Fig. 5). In order to study lamella formation, simulations must use long chains ranging from 50 to 1000 beads.[34,38,61,67,79–86] We note that CG models without an angle-dependent potential between successive bonds in the chain[64,65] do not result in the formation of lamellar structures since these angular interactions are typically the driving force of chain folding. Experiments with PHB show that the transition from extended-chain crystals to chain-folded crystals occurs around M_w of 2000 g mol^{-1} although this can be controlled by temperature.[87] For PHB with M_w of 2000 g mol^{-1}, the crystal thickness and extended chain length were about 3.3 and 6.85 nm, respectively. For PHB with M_w of 5000 g mol^{-1}, the extended chain length is 17.28 nm, and crystal thicknesses of 3.4 and 6.5 nm were observed at low and high temperature, respectively, indicating the possibility of four and two folds per chain. It is worth noting that these molecular weights are comparable to the chain lengths accessible to simulations studies.

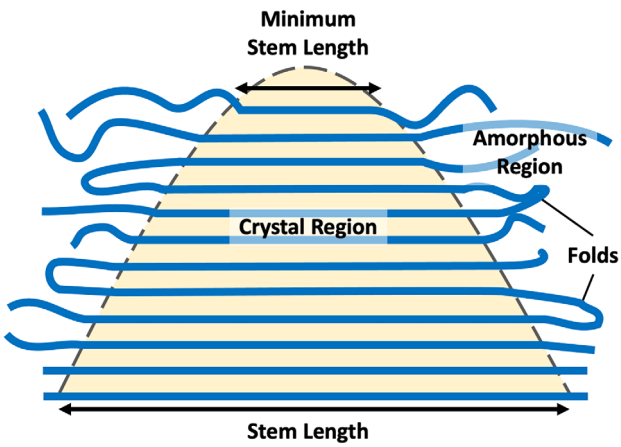

Figure 5. Schematic diagram of a lamella structure showing chain folding and stem length.

The formation of lamellae from critical nuclei was simulated using a UA model by Anwar and Schilling.[61] They found that lamella growth was precipitated by chain segments aligned to the growth front sliding in from the amorphous region. The observed lamella growth rate was found to be linear in time for early growth before transitioning to a logarithmic growth rate, which is in agreement with a CG study by Luo and Sommer.[88] Although the above studies agree on lamella growth rates, they disagree on the nature of precursor structures (the chain segments joining the lamella growth front). Anwar and Schilling[61] found that the precursor structure does not fold before joining the lamella growth front, whereas Luo and Sommer[88] found that precursor structure first fold then join the lamella growth front, only to straighten once part of the growing lamella.

Crystal lamella formation was also studied in a melt of long chains[67] using a Kremer–Grest model. The local alignment of chains was followed by rapid crystal growth in the direction perpendicular to chain orientation, leading to the formation of lamellae surrounded by amorphous regions; this observation is consistent with simulations by Luo and Sommer[88] and Yamamoto.[34] In the study by Morthomas *et al.*[67] the largest grown crystal was found to be more than three times longer than it was thick, along with 60–70% of the simulated system being crystalline.

Variability in stem lengths (Fig. 5) has been observed in crystal formation and growth[81,83] and even two nuclei of similar size can have differing stem length distributions.[84] Hall *et al.*[84] observed that crystals had a tapered growth front with a minimum stem length of three carbon atoms. In a study of long chains consisting of 1000 UAs, Verho *et al.*[85] also found that the crystal edge formed a parabolic shape; however, they found a minimum stem length of approximately 4 nm, which is much larger than the minimum stem length suggested by Hall *et al.* Tapering at the edge of lamellae can also be seen in simulation snapshots of a 100-bead CG model,[86] and interestingly they also obtain an inverse relationship between stem length and melting temperature – a relationship observed in experiments. They note that the chains studied are weakly entangled and mostly disentangled during the formation of lamellae.

Formation of microfibrils and spherulites and degree of crystallinity

Lamellae form microfibrils which further assemble into spherulites (Fig. 1). Microfibrils are arranged so that the axis corresponding to the PHB unit cell *a*-axis is parallel to the radius of the spherulite.[89] The reported values of microfibril width vary between 5 and 50 nm,[87,90] and the spherulitic structures grow up to several millimetres.[91] Spherulite growth starts with a nucleation centre, which is either an embryo created by the entanglement of polymer chains (homogeneous nucleation) or at a nucleation centre such as impurity or filler (heterogeneous nucleation), with the microfibrils branching outwards in a radial manner. Under polarised optical microscopy, this arrangement results in a so-called Maltese cross pattern; however, other arrangements such as concentric rings might be formed.[92] The

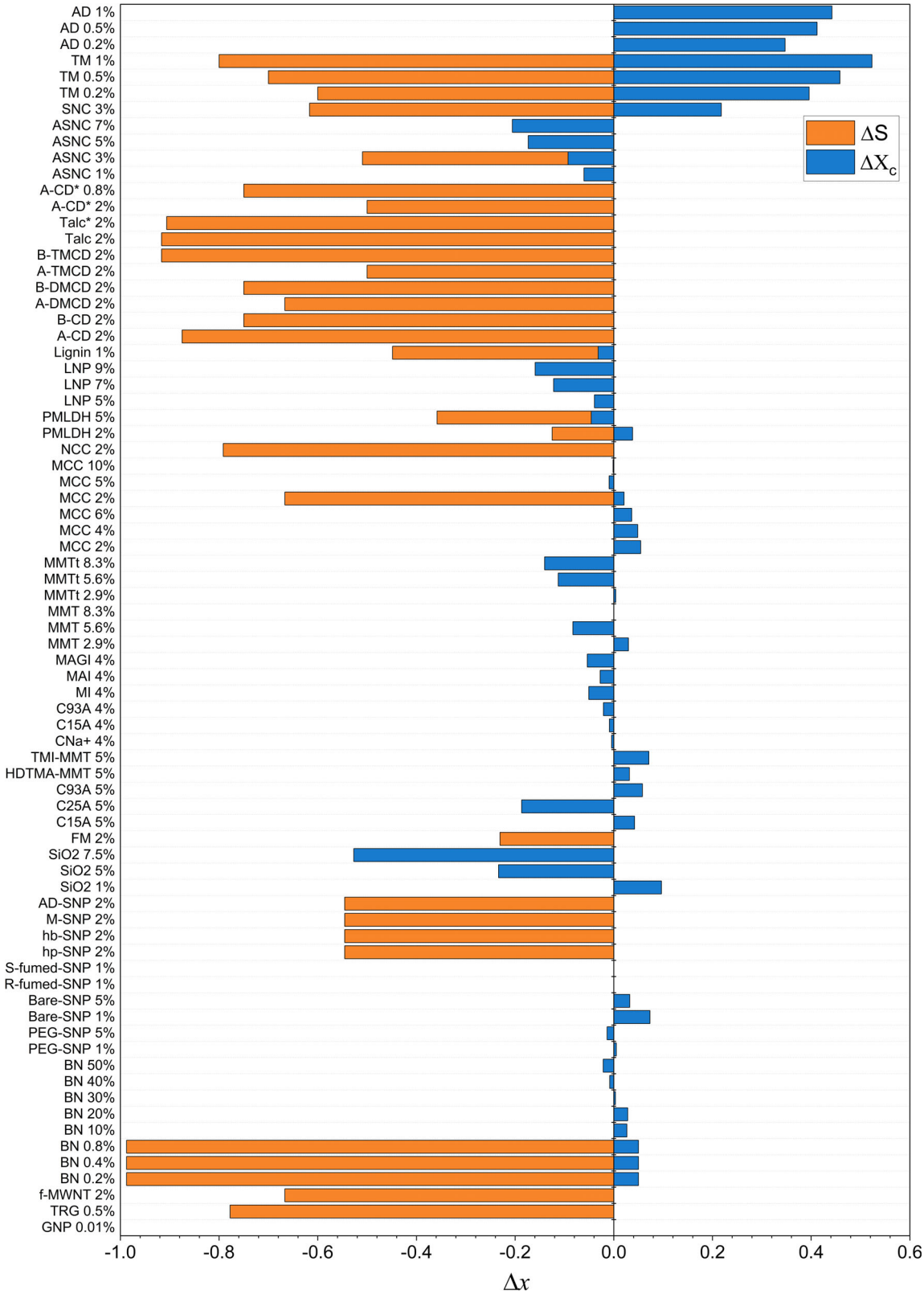

Figure 6. Legend on next page.

degree of spherulite perfection is dependent on temperature.[87] Accordingly, structures of decreased regularity are observed at temperatures closer to the melting point T_m. Furthermore, at these temperatures, dendrites and needle-like crystal aggregates were detected at the initial stage of the crystallisation process. Both phenomena occur as a result of the temperature-dependent

segmental motion of the polymer chains. At low supercooling, the diffusion coefficient of individual polymer chains is greater compared to lower temperatures and the creation of stable crystalline structures on various length scales is prevented.[87]

Disordered polymer regions

The areas between the microfibrils are filled by a disordered amorphous phase[93] that transitions into a rigid amorphous phase in the immediate vicinity of the polymer crystals (Fig. 1). Because of the steric constraints resulting from part of the polymer chain being incorporated in the crystallites, the rigid amorphous phase is in the glassy state,[94–96] characterised by a different conformation of the polymer chains compared to mobile amorphous phase.[95,97–100] The fraction of rigid amorphous phase is dependent on the internal properties of polymer chains (flexibility), crystallisation conditions (temperature) and properties of the created crystals (size, degree of irregularity of the lamellar crystal stacking, crystal morphology).[101,102]

Overall, the amorphous region is characterised by the presence of only short-range order, and this irregular arrangement results in density changes compared to a crystalline region. For PHB the densities are 1.18 and 1.26 g cm^{-3} for amorphous and crystalline regions,[15] respectively. It is this amorphous region that leads to the polymer elasticity, flexibility and low tensile strength.[103] The glass transition temperature of PHB is in the range 0–15 °C,[15,89,104–106] and was found to be positively correlated with X_c[89] and M_w up to 2000 g mol^{-1},[87] reaching a plateau and showing no further change above this threshold. The amorphous region is very important when considering transport of molecular species (water, additives, etc.) in polymer films.[107] Molecular transport takes place almost exclusively in the amorphous region due to its less defined molecular structure and accordingly higher free volume than the crystalline phase, leading to a decrease in barrier properties of the material. Therefore, a fine balance between barrier properties and mechanical properties needs to be considered while designing the packaging material for a given application.

INTRODUCING FILLER PARTICLES TO CHANGE CRYSTALLINITY AND MECHANICAL PROPERTIES

It is generally assumed that fillers act as nucleants for polymer crystallisation; however, the relationship between filler addition and polymer crystallisation (on the lamellar and spherulite level) is not fully understood. In this section, we discuss the current understanding of the effect of filler addition on polymer nucleation, degree of crystallisation, spherulite size and mechanical properties.

Effect of surfaces on polymer nucleation

Molecular modelling typically represents filler surfaces as a smooth-wall potential (such as a Lennard-Jones potential) or as an atomistic surface, and crystallisation has been observed at both of these types of surfaces. In general, nucleation occurs at the surface[59,108] although homogeneous nucleation is also observed.[108] The strength of the interaction between the polymer and the surface has been shown to influence nucleation. A weakly attractive surface enables nucleation at the surface to occur at a higher temperature than in the bulk,[108] which is due to a decreased entanglement weight at the surface. Similarly, an MC study[109] found that a weakly attractive surface yields enhanced nucleation compared to the bulk, although further increasing the interaction strength reduced the crystallisation rate eventually inhibiting it, which was attributed to reduced chain mobility due to the strong surface adsorption.

Experimental work has indicated that epitaxial matching plays a role in PHB crystallisation[110–112] and a simulation study of UA chains found that a poorer lattice match resulted in longer induction times.[113] Nucleation at the surface is also supported by a GISAXS study that observed a surface-bound lamella layer with chains aligned with the surface.[114] Simulations have found that lamellae grow with chains aligned with the surface,[79,115] and that the edge tapers into the amorphous region with the thickest stems situated at the surface.[79]

Filler particles are often functionalised or grafted to aid their dispersion in the polymer matrix. Simulation studies have investigated nucleation in grafted systems, and it was found that grafting suppresses nucleation at the surface,[108,116,117] and for a high enough grafting density, nucleation is observed only in the bulk.[108] However, other studies found that higher grafting densities result in shorter induction times, and that increasing grafting density changes the nucleation mechanism and crystal orientation.[118–120]

Crystallisation near filler particles of various shapes and sizes has been simulated, including one-dimensional cylindrical shapes,[117,121] two-dimensional platelets[121] and spherical nanoparticles.[122] An MC study on the effect of nanofiller dimension on crystallinity[121] demonstrated that filler dimension influences the crystallisation rate and orientation. Confinement effects (when the geometrical constraints on the system are of a length scale similar to that of the polymer chain) may also be important, particularly if the filler concentration is high or if fillers are porous. Polymer material in filler pores or in the gaps between filler particles will exhibit properties, such as the glass transition temperature, that are different from those of the polymer in an unconfined region. Nucleation tends to be suppressed in confined systems, including ultrathin films[109,114,115] and nanopores,[118,123] and is attributed to a reduction in chain mobility.[115,118]

Effect of fillers on degree of crystallinity and spherulites

While simulations have provided insight into how fillers may influence crystallisation, the picture from experimental studies is less

Figure 6 Changes in crystallinity, X_c, and spherulite size, S, for filled samples with filler weight percent compared to pure PHB. The filler types are graphene nanoparticles (GNP),[125] thermally reduced graphene (TRG);[126] carboxyl-functionalized multi-walled carbon nanotubes (f-MWNT);[127] boron nitride (BN);[128,129] poly(ethylene glycol)-grafted silica nanoparticles (PEG-SNP), bare silica nanoparticles (Bare-SNP), R812 fumed silica nanoparticles (R-fumed-SNP), S5130 fumed silica nanoparticles (S-fumed-SNP);[130,131] hydrophilic silica nanoparticles (hp-SNP), hydrophobic silica nanoparticles (hb-SNP), methyl methacrylate-treated silica nanoparticles (M-SNP), amidoamine-treated silica nanoparticles (AD-SNP);[132] silica (SiO_2);[133] fluoromica (FM),[134] montmorillonite (MMT);[135] MMT treated with 25–30 wt% methyldihydroxyethyl hydrogenated tallow ammonium (MMTt);[135] Cloisite 15A, 25A, 93A, Na^+ – C15A, C25A, C93A, CNa+, respectively;[136] hexadecyltrimethylammonium bromide-modified montmorillonite (HDTMA-MMT); transition metal ions ($ZnNO_3$)-modified montmorillonite (TMI-MMT);[137] CNa+ modified with tributylhexadecylphosphonium bromide (MI), H_2SO_4 (MAI) and dimethyloctadecylchlorosilane (MAGI);[138] microcrystalline cellulose (MCC);[139,140] nanocrystalline cellulose (NCC);[140] poly(ethylene glycol) phosphonate-modified layered double hydroxides (PMLDH);[141,142] lignin;[143] lignin nanoparticles (LNP);[144] α-cyclodextrin (A-CD*,[145] A-CD[146]), β-cyclodextrin (B-CD);[146] 2,6-di-O-methyl-α-cyclodextrin (A-DMCD), 2,6-di-O-methyl-β-cyclodextrin (B-DMCD), 3,6-tri-O-methyl-α-cyclodextrin(A-TMCD), 2,3,6-tri-O-methyl-β-cyclodextrin (B-TMCD);[146] talc*,[145] talc;[146] inclusion complex of 0.8% A-CD and PHB (A-CD* 0.8%);[145] acetylated starch nanocrystals (ASNC), starch nanocrystals (SNC);[147] and thymine and adonitol (TM, AD).[112] Filler properties are given in the supporting information (Table S1) and in the original papers.

clear. We think it is informative to consider what is happening to the number density and size of spherulites in the data reported for filled PHB samples. In general, we found that PHB–filler composites have smaller but more numerous spherulites compared to pure PHB. This indicates that the filler acts as a nucleating agent in the composite, which is consistent with the simulation studies that observed that surfaces induce polymer nucleation. As is common in Avrami analysis, we assume that the degree of crystallinity of the sample should be proportional to the number and volume of the spherulites, with the number of spherulites expected to be proportional to filler concentration. A summary of the degree of crystallinity, X_c, and median spherulite size, S, for various fillers in PHB is presented in the supporting information (Table S1).

We note that X_c varies greatly for both filled PHB composites and for pure PHB samples due to variations in the polymer properties, the processing method, etc. In order to decouple these effects, we calculated the change in crystallinity and change in spherulite size of the filled samples compared to a corresponding pure PHB sample from the same literature source. The changes in X_c and S are defined as

$$\Delta x = \frac{x_f - x_0}{x_0}$$

where x refers to X_c or S, and the subscripts 'f' and '0' refer to filled samples or pure PHB, respectively.

Figure 6 presents the change in crystallinity, ΔX_c, of a range of filled PHB samples from the literature. It is clear that ΔX_c varies greatly with addition of various fillers, and there is no consistent effect of filler addition on ΔX_c. These differences may be connected to the nature of the filler surface and its interaction with the polymer, but without systematically varying filler surface properties it is difficult to isolate surface effects.

Figure 6 also shows the change in S for filler addition, denoted ΔS. In all cases, S decreases or stays the same with the addition of fillers compared to pure PHB sample. Where both S and X_c are reported, we have estimated the spherulite number density, using the approximation that X_c is proportional to the number and volume of spherulites, and we found that the number of spherulites increases with filler concentration. Three main factors are thought to influence crystallisation behaviour upon increasing filler concentration: an increase in the number of nucleation sites, increased filler aggregation and reduced polymer chain mobility. The filler surface properties will influence both the nucleation and filler aggregation as the interaction of the filler with the polymer matrix can affect the dispersion of the filler particles. Therefore, the overall behaviour of the filler in the system is dependent on the prevailing nature of intermolecular interactions that influence the changes in X_c and S of the system.[124]

Mechanical properties of PHB–filler systems and correlation with crystallinity

The mechanical properties are influenced by the fraction of amorphous, crystalline and interfacial regions, and the distribution and size of the spherulites in the polymer matrix. Pure PHB typically consists of large spherulites that result in brittleness, with the large spherulites exhibiting the tendency to crack. This happens because molecular conformation changes are difficult due to the retarded movement of the molecular segments by the continuous crystallisation phase.[148] Systems with smaller or incomplete spherulites do not show the same tendency to crack. As discussed in the previous section, fillers act as nucleating agents and in general lead to the creation of spherulites of smaller size compared to pristine PHB. It is therefore expected that mechanical properties show a dependence on changes in spherulite size upon filler addition. However, although most experimental

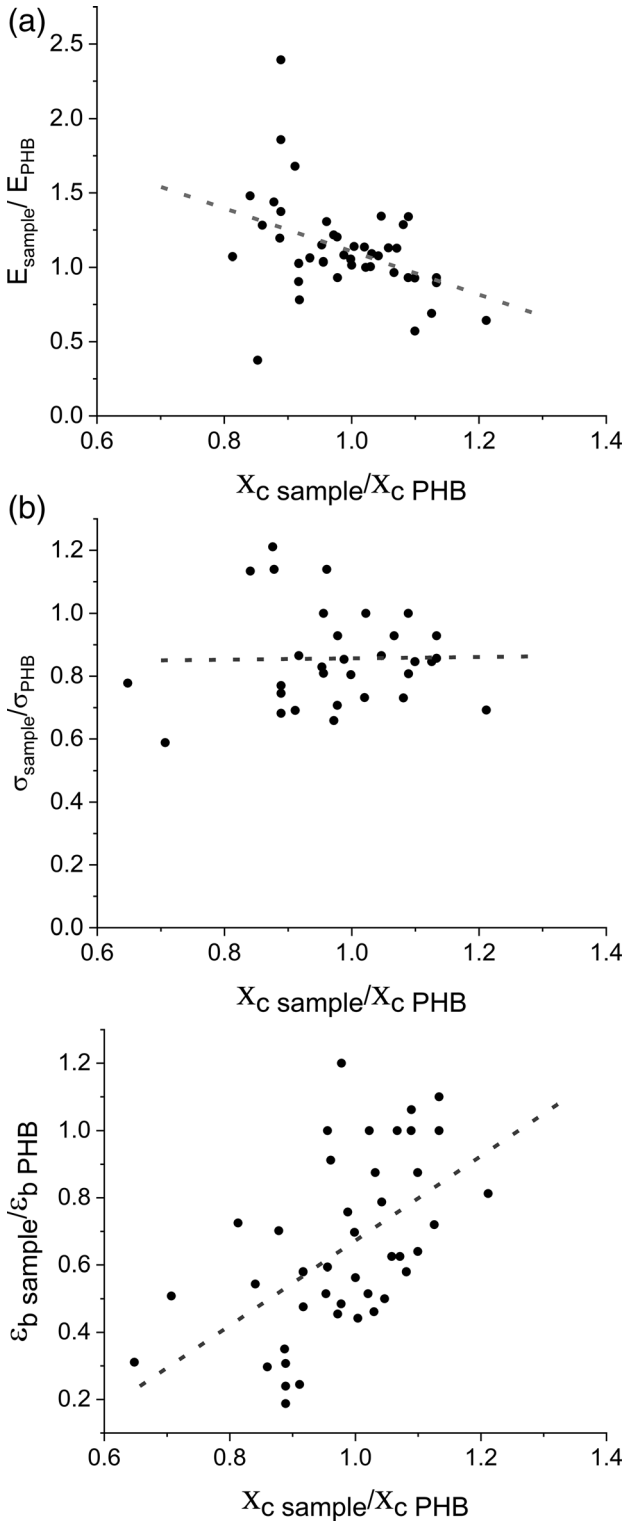

Figure 7. Changes in normalised mechanical properties of PHB–filler composites with changes in the degree of crystallinity due to filler addition: (a) Young's modulus E; (b) tensile strength σ; (c) elongation at break ε_b. Dashed lines are guides to the eye. The literature data for this figure are summarised in the supporting information (Table S2) and citations therein.[135,137,144,151–158]

studies of the mechanical properties of PHB–filler systems do provide data about the degree of crystallinity, information about spherulite size is less available. When such information is available, in general no clear correlation between spherulite size and mechanical properties for PHB composites is reported.[131]

The mechanical properties (tensile properties) of PHB–filler systems, taken from literature sources, are presented in the supporting information (Table S2). The mechanical properties presented in Table S2 – Young's modulus (E), tensile strength (σ) and strain at break (ε_b) – are defined in Fig. 2. Since the mechanical properties and X_c are dependent on the processing method and the molecular weight of PHB,[149,150] the present analysis uses normalised values, i.e. the values of the mechanical properties and X_c of the filled samples were divided by the values obtained for the pure PHB used in each experiment. Figure 7 presents the normalised values of Young's modulus, tensile strength and strain at break as a function of normalised X_c for PHB–filler systems. Overall, introducing fillers results in a decrease in ε_b and in variations of Young's modulus dependent on the filler chemistry. Figure 7(a) shows a weak correlation between E and X_c, with E decreasing with increasing X_c. As shown in Fig. 7(b), σ does not correlate with X_c and there is a positive correlation between ε_b and X_c (Fig. 7(c)).

Figure 7 presents weak and apparently counterintuitive correlations between mechanical properties and degree of crystallinity. In pristine/unfilled polymer systems, an increase in the degree of crystallinity usually leads to an increase in Young's modulus and a reduction in strain at break. However, in polymer–filler systems, the properties of the pure polymer and the filler, as well as changes in polymer matrix induced by the presence of the filler need to be considered. Due to this additional complexity, it is clear that a simple causal link between degree of crystallinity and mechanical properties cannot be established as many more factors are at play. Referring back to Fig. 6, we see that the dominant effect of filler addition is to decrease spherulite size. This perhaps provides a clue to the behaviour seen in Figs 7(a) and (c). It is possible that the modified microstructure of filled systems, with increased number density of crystalline–amorphous interfaces, might be responsible for the trends, and merits further consideration in future work.

CONCLUSIONS

PHB-based plastic packaging materials derived from microbial fermentation processes are a promising candidate for replacing petroleum-based counterparts. However, their undesirable properties such as low thermal stability and high degree of crystallinity (resulting in stiffness and brittleness) need to be minimised prior to industrial implementation, balanced with the need for good barrier properties. Despite the many literature studies of crystallisation in pure PHB, the relationship between the crystallinity, M_w of the polymer, and processing method is not well understood. This in turn results in lack of control of the final product, making it unfeasible for commercial applications.

The mechanical properties of PHB can be adjusted by the addition of additives, such as filler particles. We have found that, in general, fillers act as nucleants and induce the formation of a higher number of spherulites of smaller size without significant or systematic changes in the overall degree of crystallinity compared to pure PHB. The filler properties play a significant role in controlling PHB crystallisation, and there should be further work to investigate the role of the filler surface–polymer interactions in nucleation of PHB. In addition, we suggest a need for future experimental studies to include the spherulite size distribution in addition to degree of crystallinity. Without this information, it is challenging to provide an unambiguous trend in the system behaviour upon introducing various fillers to the system, partly due to variations in processing methods, the presence of more than one additive and variations in filler surface properties, shape and size.

Molecular simulations have provided molecular-level insight into the initial stages of polymer crystallisation, which are currently experimentally inaccessible. However, these are not able to reach the time and length scales necessary to model spherulitic formation and growth. Recently, simulations have been used to study the effects of filler particles on nucleation. However, the number of studies is not extensive and more studies are needed to understand how the filler surface properties, such as epitaxy, surface chemistry (filler–polymer interaction strength), surface functionalisation, including grafting and sizing, and filler geometry, affect polymer nucleation and hence crystal growth.

While it is difficult to directly predict the composite properties based on a comparison of simulation and experiment, simulations can provide useful insight into how surface properties influence polymer nucleation. The nucleation mechanism can be used to control the degree of crystallinity and spherulite size, which can be measured experimentally. Therefore, a combination of carefully planned simulations and experiments will help to elucidate the link between filler surface properties and composite structure and properties, thus facilitating prediction and design of composite materials. We also note that there is a lack of molecular simulations specifically concerning PHB, and it would be of interest to study the role of specific interactions, such as hydrogen bonding and electrostatics, in PHB nucleation.

We have demonstrated the need for more systematic or wide-ranging studies that aim to strengthen the understanding of how the degree of crystallinity and spherulite size affect the mechanical properties of PHB-based films. Further, these studies should be extended to address the effect of additives in the system, processing routes and storage conditions to account for physical ageing and secondary crystallisation.

ACKNOWLEDGEMENTS

This work was funded by an Innovate UK Smart Sustainable Plastic Packaging grant (NE/V010603/1).

DATA AVAILABILITY STATEMENT

All data underpinning this publication are openly available from the University of Strathclyde KnowledgeBase at: https://doi.org/10.15129/36891b98-7209-409b-b7f9-8f68ac119ed8.

SUPPORTING INFORMATION

Supporting information may be found in the online version of this article.

REFERENCES

1 Rhodes CJ, *Sci Prog* **101**:207–260 (2018).
2 Pivokonsky M, Cermakova L, Novotna K, Peer P, Cajthaml T and Janda V, *Sci Total Environ* **643**:1644–1651 (2018).
3 De-la-Torre GE, *J Food Sci Technol* **57**:1601–1608 (2020).
4 Gasperi J, Wright SL, Dris R, Collard F, Mandin C, Guerrouache M *et al.*, *Curr Opin Environ Sci Heal* **1**:1–5 (2018).
5 Poore J and Nemecek T, *Science (80-)* **360**:987–992 (2018).

6 Moult JA, Allan SR, Hewitt CN and Berners-Lee M, *Food Policy* **77**:50–58 (2018).
7 Philip S, Keshavarz T and Roy I, *J Chem Technol Biotechnol* **82**:233–247 (2007).
8 Rehm BHA, *Biochem J* **376**:15–33 (2003).
9 Steinbüchel A, Polyhydroxyalkanoic acids, in *Biomaterials: Novel Materials from Biological Sources*, ed. by Byrom D. Palgrave Macmillan, London, UK, pp. 124–213 (1991).
10 Steinbachel A and Valentin HE, *FEMS Microbiol Lett* **128**:219–228 (1995).
11 Hazer B and Steinbüchel A, *Appl Microbiol Biotechnol* **74**:1–12 (2007).
12 Sharma V, Sehgal R and Gupta R, *Polymer (Guildf)* **212**:123161 (2021).
13 Puppi D, Pecorini G and Chiellini F, *Bioengineering* **6**:108 (2019).
14 Corre Y-M, Bruzaud S, Audic J-L and Grohens Y, *Polym Test* **31**:226–235 (2012).
15 Roohi ZMR and Kuddus M, *Polym Adv Technol* **29**:30–40 (2018).
16 Singh M, Kumar P, Ray S and Kalia VC, *Indian J Microbiol* **55**:235–249 (2015).
17 Sodian R, Sperling JS, Martin DP, Egozy A, Stock U, Mayer JE *et al.*, *Tissue Eng* **6**:183–188 (2000).
18 Muthuraj R, Valerio O and Mekonnen TH, *Int J Biol Macromol* **187**:422–440 (2021).
19 Thellen C, Cheney S and Ratto JA, *J Appl Polym Sci* **127**:2314–2324 (2013).
20 Gao Y, Kong L, Zhang L, Gong Y, Chen G, Zhao N *et al.*, *Eur Polym J* **42**:764–775 (2006).
21 Dingler C, Dirnberger K and Ludwigs S, *Macromol Rapid Commun* **40**:1800601 (2019).
22 Deng Y, Zhao K, Zhang X, Hu P and Chen G-Q, *Biomaterials* **23**:4049–4056 (2002).
23 Zheng Z, Bei F-F, Tian H-L and Chen G-Q, *Biomaterials* **26**:3537–3548 (2005).
24 Horowitz DM, Clauss J, Hunter BK and Sanders JKM, *Nature* **363**:23 (1993).
25 de Koning GJM and Lemstra PJ, *Polymer (Guildf)* **33**:3292–3294 (1992).
26 Sanders JKM, *Chem Soc Rev* **22**:1–7 (1993).
27 Pearce R, Brown GR and Marchessault RH, *Polymer (Guildf)* **35**:3984–3989 (1994).
28 Vroman I and Tighzert L, *Materials (Basel)* **2**:307–344 (2009).
29 Porter M and Yu J, *J Biomater Nanobiotechnol* **2**:301–310 (2011).
30 Biddlestone F, Harris A, Hay JN and Hammond T, *Polym Int* **39**:221–229 (1996).
31 Hong S-G, Gau T-K and Huang S-C, *J Therm Anal Calorim* **103**:967–975 (2011).
32 Seoane IT, Manfredi LB and Cyras VP, *J Appl Polym Sci* **135**:46016 (2018).
33 El-Hadi A, Schnabel R, Straube E, Müller G and Riemschneider M, *Macromol Mater Eng* **287**:363 (2002).
34 Yamamoto T, *Polymer (Guildf)* **50**:1975–1985 (2009).
35 Tretinnikov ON and Zagorskaya SA, *J Appl Spectrosc* **79**:521–526 (2012).
36 Frenkel D and Smit B, *Understanding Molecular Simulations: From Algorithms to Applications*. Elsevier Science Publishers, Amsterdam, The Netherlands (2001).
37 Allen MP and Tildesley DJ, *Computer Simulations of Liquids*. Oxford University Press, Oxford, UK (2017).
38 Vettorel T and Meyer H, *J Chem Theory Comput* **2**:616–629 (2006).
39 Karimi-Varzaneh HA, van der Vegt NFA, Müller-Plathe F and Carbone P, *ChemPhysChem* **13**:3428–3439 (2012).
40 Abrams CF and Kremer K, *Macromolecules* **36**:260–267 (2003).
41 Reith D, Meyer H and Müller-Plathe F, *Macromolecules* **34**:2335–2345 (2001).
42 Kremer K and Grest GS, *J Chem Phys* **92**:5057–5086 (1990).
43 Everaers R, Karimi-Varzaneh HA, Fleck F, Hojdis N and Svaneborg C, *Macromolecules* **53**:1901–1916 (2020).
44 Svaneborg C and Everaers R, *Macromolecules* **53**:1917–1941 (2020).
45 Ellar D, Lundgren DG, Okamura K and Marchessault RH, *J Mol Biol* **35**:489–502 (1968).
46 Marchessault RH, Coulombe S, Morikawa H, Okamura K and Revol JF, *Can J Chem* **59**:38–44 (1981).
47 Sudesh K, Abe H and Doi Y, *Prog Polym Sci* **25**:1503–1555 (2000).
48 Laycock B, Halley P, Pratt S, Werker A and Lant P, *Prog Polym Sci* **38**:536–583 (2013).
49 Yokouchi M, Chatani Y, Tadokoro H, Teranishi K and Tani H, *Polymer (Guildf)* **14**:267–272 (1973).
50 Okamura K and Marchessault RH, X-ray structure of poly-β-hydroxybutyrate, in *Conformation of Biopolymers*, ed. by Ramachandran GN. Academic Press, London, UK, pp. 709–720 (1967).
51 Cobntbekt J and Mabchessault RH, *J Mol Biol* **71**:735–756 (1972).
52 Furukawa T, Sato H, Murakami R, Zhang J, Noda I, Ochiai S *et al.*, *Polymer (Guildf)* **47**:3132–3140 (2006).
53 Perret E, Reifler FA, Gooneie A and Hufenus R, *Polymer (Guildf)* **180**:121668 (2019).
54 Wang S, Chen W, Xiang H, Yang J, Zhou Z and Zhu M, *Polymers (Basel)* **8**:273 (2016).
55 Glova AD, Falkovich SG, Dmitrienko DI, Lyulin AV, Larin SV, Nazarychev VM *et al.*, *Macromolecules* **51**:552–563 (2018).
56 Kyles RE and Tonelli AE, *Macromolecules* **36**:1125–1131 (2003).
57 Glova AD, Larin SV, Nazarychev VM, Karttunen M and Lyulin SV, *Macromolecules* **53**:29–38 (2020).
58 Fujiwara S and Sato T, *Phys Rev Lett* **80**:991–994 (1998).
59 Waheed N, Ko MJ and Rutledge GC, *Polymer (Guildf)* **46**:8689–8702 (2005).
60 Yi P and Rutledge GC, *J Chem Phys* **135**:024903 (2011).
61 Anwar M and Schilling T, *Polymer (Guildf)* **76**:307–312 (2015).
62 Shakirov T and Paul W, *Phys Rev E* **97**:42501 (2018).
63 Yi P, Locker CR and Rutledge GC, *Macromolecules* **46**:4723–4733 (2013).
64 Hoy RS and Karayiannis NC, *Soft Matter Phys* **88**:1–7 (2013).
65 Karayiannis NC, Foteinopoulou K and Laso M, *Phys Rev Lett* **103**:045703 (2009).
66 Karayiannis NC and Laso M, *Phys Rev Lett* **100**:050602 (2008).
67 Morthomas J, Fusco C, Zhai Z, Lame O and Perez M, *Phys Rev E* **96**:052502 (2017).
68 Wang H and Tashiro K, *Macromolecules* **49**:581–594 (2016).
69 Phongtamrug S and Tashiro K, *Macromolecules* **52**:2995–3009 (2019).
70 Iwata T and Tanaka T, Manufacturing of PHA as fibers, in *Plastics from Bacteria*, Vol. **14**, ed. by Chen GG-Q. Springer, Berlin, Germany, pp. 257–282 (2010).
71 Iwata T, Sato S, Park JW and Tanaka T, *In International Symposium on Biological Polyesters*:101 (2008).
72 Sato S, Tanaka T, Yoshida Y and Iwata T, *Polym Prepr Jpn* **56**:56–63 (2007).
73 Furukawa T, Sato H, Murakami R, Zhang J, Duan YX, Noda I *et al.*, *Polym Prepr Jpn* **54**:3593 (2005).
74 Sato H, Dybal J, Murakami R, Noda I and Ozaki Y, *J Mol Struct* **744–747**:35–46 (2005).
75 Yi P and Rutledge GC, *J Chem Phys* **131**:1–11 (2009).
76 Anwar M, Turci F and Schilling T, *J Chem Phys* **139**:214904 (2013).
77 Takeuchi H, *J Chem Phys* **109**:5614–5621 (1998).
78 Miura T, Kishi R, Mikami M and Tanabe Y, *Phys Rev E* **63**:061807 (2001).
79 Yamamoto T, *Polymer (Guildf)* **45**:1357–1364 (2004).
80 Luo C and Sommer JU, *Phys Rev Lett* **112**:195702 (2014).
81 Sommer JU and Luo C, *J Polym Sci B Polym Phys* **48**:2222–2232 (2010).
82 Paajanen A, Vaari J and Verho T, *Polymer (Guildf)* **171**:80–86 (2019).
83 Zhai Z, Fusco C, Morthomas J, Perez M and Lame O, *ACS Nano* **13**:11310–11319 (2019).
84 Hall KW, Sirk TW, Percec S, Klein ML and Shinoda W, *Polymers (Basel)* **12**:447 (2020).
85 Verho T, Paajanen A, Vaari J and Laukkanen A, *Macromolecules* **51**:4865–4873 (2018).
86 Meyer H and Müller-Plathe F, *J Chem Phys* **115**:7807–7810 (2001).
87 Androsch R, Radusch H-J and Funari SS, *Eur Polym J* **43**:4961–4974 (2007).
88 Luo C and Sommer JU, *Macromolecules* **44**:1523–1529 (2011).
89 dos Santos AJ, Oliveira Dalla Valentina LV, Hidalgo Schulz AA and Tomaz Duarte MA, *Ing y Cienc* **13**:269–298 (2017).
90 Abe H, Kikkawa Y, Iwata T, Aoki H, Akehata T and Doi Y, *Polymer (Guildf)* **41**:867–874 (2000).
91 Barham PJ, Keller A, Otun EL and Holmes PA, *J Mater Sci* **19**:2781–2794 (1984).
92 Crist B and Schultz JM, *Prog Polym Sci* **56**:1–63 (2016).
93 Hoffman JD, Davis GT and Lauritzen JI, *Treatise Solid State Chem* 497–614 (1976). https://link.springer.com/chapter/10.1007/978-1-4684-2664-9_7
94 Alsleben M and Schick C, *Thermochim Acta* **238**:203–227 (1994).
95 Schick C, Wurm A and Mohammed A, *Thermochim Acta* **396**:119–132 (2003).
96 Thomas D, Zhuravlev E, Wurm A, Schick C and Cebe P, *Polymer (Guildf)* **137**:145–155 (2018).

97 Morin FG and Marchessault RH, *Macromolecules* **25**:576–581 (1992).
98 El-Taweel SH, Höhne GWH, Mansour AA, Stoll B and Seliger H, *Polymer (Guildf)* **45**:983–992 (2004).
99 Hutníková M and Fričová O, *Acta Phys Pol A* **129**:388–393 (2016).
100 Di Lorenzo ML, Gazzano M and Righetti MC, *Macromolecules* **45**:5684–5691 (2012).
101 Heberer DP, Cheng SZD, Barley JS, Lien SHS, Bryant RG and Harris FW, *Macromolecules* **24**:1890–1898 (1991).
102 Androsch R and Wunderlich B, *Polymer (Guildf)* **46**:12556–12566 (2005).
103 Roberts JD and Caserio MC, *Basic Principles of Organic Chemistry*. WA Benjamin, San Francisco, CA, pp. 1419–1459 (1977).
104 Bugnicourt E, Cinelli P, Lazzeri A and Alvarez V, *Express Polym Lett* **8**:791–808 (2014).
105 Harrison STL, Chase HA, Amor SR, Bonthrone KM and Sanders JKM, *Int J Biol Macromol* **14**:50–56 (1992).
106 dos Santos RD, Calil MR, Fassina Guedes C das G and Rodrigues TC, *J Polym Environ* **12**:239–245 (2004).
107 Van Etten EA, Ximenes ES, Tarasconi LT, Garcia ITS, Forte MMC and Boudinov H, *Thin Solid Films* **568**:111–116 (2014).
108 Luo C, Kröger M and Sommer JU, *Polymer (Guildf)* **109**:71–84 (2017).
109 Qiu X, Zhang Y, Wu H, Yang R, Yang J, Liu R *et al.*, *Polym Int* **68**:218–224 (2019).
110 Organ SJ and Barham PJ, *J Mater Sci* **27**:3239–3242 (1992).
111 Vesely D and Ronca G, *J Microsc* **201**:137–143 (2001).
112 Ma H, Wei Z, Zhou S, Zhu H, Tang J, Yin J *et al.*, *Int J Biol Macromol* **165**:1562–1573 (2020).
113 Bourque AJ, Locker CR and Rutledge GC, *J Phys Chem B* **121**:904–911 (2017).
114 Asada M, Jiang N, Sendogdular L, Gin P, Wang Y, Endoh MK *et al.*, *Macromolecules* **45**:7098–7106 (2012).
115 Ma Y, Hu W and Reiter G, *Macromolecules* **39**:5159–5164 (2006).
116 Glova AD, Falkovich SG, Larin SV, Mezhenskaia DA, Lukasheva NV, Nazarychev VM *et al.*, *Polym Int* **65**:892–898 (2016).
117 Zhang S, Ming Y, Wei Y, Hao T, Nie Y and Zhou Z, *J Appl Polym Sci* **138**:8–10 (2021).
118 Ma Y, Hu W, Hobbs J and Reiter G, *Soft Matter* **4**:540–543 (2008).
119 Hao T, Zhou Z, Nie Y, Zhu L, Wei Y and Li S, *Polymer (Guildf)* **100**:10–18 (2016).
120 Hao T, Zhou Z, Nie Y, Wei Y, Gu Z and Li S, *Polymer (Guildf)* **123**:169–178 (2017).
121 Gu Z, Yang R, Yang J, Qiu X, Liu R, Liu Y *et al.*, *Comput Mater Sci* **147**:217–226 (2018).
122 Zhang D and Meyer H, *J Polym Sci B Polym Phys* **45**:2161–2166 (2007).
123 Ming Y, Zhou Z, Zhang S, Wei Y, Hao T and Nie Y, *Polymer (Guildf)* **206**:122818 (2020).
124 Jiang N and Abe H, *J Appl Polym Sci* **132**:1–9 (2015).
125 Miloaga DG, H-AA H, Misra M and Drzal LT, *J Appl Polym Sci* **106**:2548–2558 (2007).
126 Jing X and Qiu Z, *Ind Eng Chem Res* **51**:13686–13691 (2012).
127 Xu C and Qiu Z, *Polym Adv Technol* **22**:538–544 (2011).
128 Puente JAS, Esposito A, Chivrac F and Dargent E, *J Appl Polym Sci* **128**:2586–2594 (2013).
129 Li Z, Kong J, Han L, Zhang H and Dong L, *Polym Bull* **75**:1651–1666 (2018).
130 Lan C-H and Sun Y-M, *Mater Chem Phys* **199**:88–97 (2017).
131 Lan C-H and Sun Y-M, *J Polym Res* **25**:121 (2018).
132 Hong S-G and Huang S-C, *J Polym Res* **22**:61 (2015).
133 Martinez Martinez Toledo AL, da Rocha Rodrigues EJ, de Paula Cavalcante M, Dutra Filho JC and Ines Bruno Tavares M, *J Thermoplast Compos Mater*:1–14 (2020). doi:10.1177/0892705720935939
134 Maiti P, Batt CA and Giannelis EP, *Biomacromolecules* **8**:3393–3400 (2007).
135 Isa MRM, Hassan A, Nordin NA, Thirmizir MZA and Ishak ZAM, *High Perform Polym* **32**:192–200 (2020).
136 D'Amico DA, Manfredi LB and Cyras VP, *Thermochim Acta* **544**:47–53 (2012).
137 Prakalathan K, Mohanty S and Nayak SK, *Polym Compos* **35**:999–1012 (2014).
138 D'Amico DA, Cyras VP and Manfredi LB, *Thermochim Acta* **594**:80–88 (2014).
139 Seoane IT, Fortunati E, Puglia D, Cyras VP and Manfredi LB, *Polym Int* **65**:1046–1053 (2016).
140 Chen J, Xu C, Wu D, Pan K, Qian A, Sha Y *et al.*, *Carbohydr Polym* **134**:508–515 (2015).
141 Hsu S-F, Wu T-M and Liao C-S, *J Polym Sci B Polym Phys* **44**:3337–3347 (2006).
142 Hsu S-F, Wu T-M and Liao C-S, *J Polym Sci B Polym Phys* **45**:995–1002 (2007).
143 Weihua K, He Y, Asakawa N and Inoue Y, *J Appl Polym Sci* **94**:2466–2474 (2004).
144 Lugoloobi I, Li X, Zhang Y, Mao Z, Wang B, Sui X *et al.*, *Int J Biol Macromol* **165**:3078–3087 (2020).
145 He Y and Inoue Y, *J Polym Sci B Polym Phys* **42**:3461–3469 (2004).
146 Shin K-M, Dong T, He Y and Inoue Y, *Macromol Chem Phys* **207**:755–762 (2006).
147 Zhang G, Wu D, Xie W, Wang Z and Xu C, *Carbohydr Polym* **195**:79–88 (2018).
148 Wang T, Cheng G, Ma S, Cai Z and Zhang L, *J Appl Polym Sci* **89**:2116–2122 (2003).
149 Hoffmann A, Kreuzberger S and Hinrichsen G, *Polym Bull* **33**:355–359 (1994).
150 Luo S, Grubb DT and Netravali AN, *Polymer (Guildf)* **43**:4159–4166 (2002).
151 Aydemir D and Gardner DJ, *Polym Compos* **41**:3842–3856 (2020).
152 Chen J, Wu D and Pan K, *Int J Biol Macromol* **88**:120–129 (2016).
153 Sánchez-Safont EL, Aldureid A, Lagarón JM, Gamez-Perez J and Cabedo L, *Waste Biomass Valorization* **12**:2541–2556 (2021).
154 Rajan R, Sreekumar PA, Joseph K and Skrifvars M, *J Appl Polym Sci* **124**:3357–3362 (2012).
155 Bergmann A and Owen A, *Polym Int* **52**:1145–1152 (2003).
156 Sánchez-Safont EL, Aldureid A, Lagarón JM, Gámez-Pérez J and Cabedo L, *Compos Part B Eng* **145**:215–225 (2018).
157 Araque LM, de Morais ACL, Alves TS, Azevedo JB, Carvalho LH and Barbosa R, *J Mater Res Technol* **8**:935–943 (2019).
158 Adorna J, Ventura RL, Dang VD, Doong R and Ventura J, *J Appl Polym Sci* **139**:51645 (2022).